PAPER • OPEN ACCESS

CFD-DEM study on the entrainment induced by debris flows with the HBP rheological model

To cite this article: Yu-Han Wang *et al* 2021 *IOP Conf. Ser.: Earth Environ. Sci.* **861** 072012
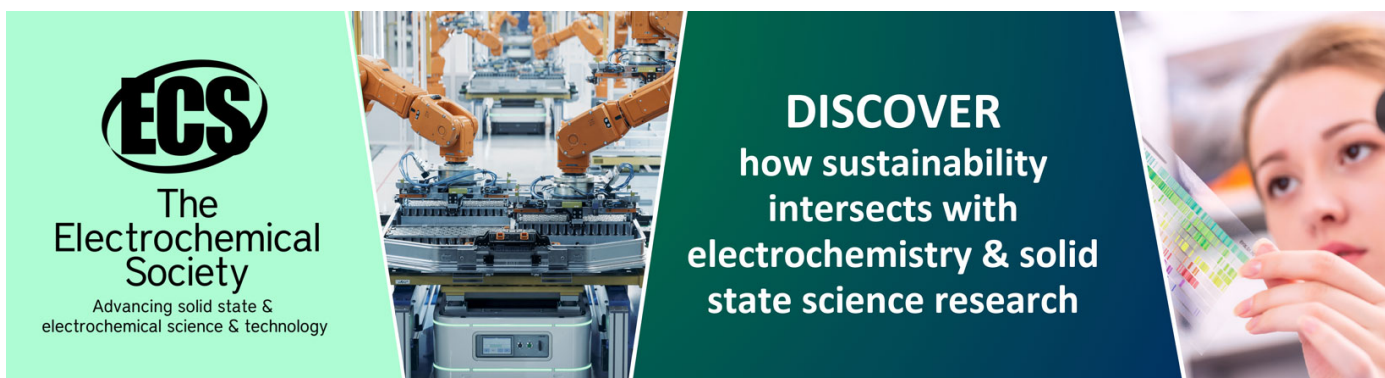
View the article online for updates and enhancements.

CFD-DEM study on the entrainment induced by debris flows with the HBP rheological model

Yu-Han Wang[a], Wu-Wei Mao[a, b*], Ping Yang[a, b], Yu Huang[a, b], Hu Zheng[a, b]

a. Department of Geotechnical Engineering, College of Civil Engineering, Tongji University, Shanghai 200092, China
b. Key Laboratory of Geotechnical and Underground Engineering, Ministry of Education, Tongji University, Shanghai 200092, China

Email: maowuwei@tongji.edu.cn

Abstract. The interaction between basal and earth-surface flows such as dam-break flows, hyper-concentration flows and debris flows, for example, entrainment and erosion, have crucial influences on their dynamic characteristics and rheological behaviour. Among these mass flows, debris flows that are able to entrain a great number of masses tend to be the most catastrophic. A fully coupled CFD-DEM technique is utilised here to evaluate the erosion effect of debris flow on the sand basal, in which basal is modelled via a non-cohesive particle assembly using DEM and debris flows are recognised as a non-Newtonian fluid. Herschel-Bulkley-Papanastasiou (HBP) rheological model is implemented to capture the viscous behaviour of debris flows. Besides, considering the gap-graded feature of basal, the traditional coarse-grain method that accounts for porosity based on particle centres may result in inaccuracy in void fraction determination. Thus, the semi-resolved method is used to determine physical fields. Morphology of the basal is updated each time step following DEM calculation cycles.

1. Introduction

Debris flows have been widely recognised as one of the catastrophic geological hazards. The initiation of development of debris flows tends to be unpredictable and speedy. Massive mixtures can be entrained during the motion of debris flows, which fairly exaggerates the damage induced by debris flows. Among composites of debris flows, larger solid particles like boulders take a crucial role in resultant destruction. Regards of the high flowing speed and damage of debris flows, experiment studies were mostly conducted with the centrifuge model and large-scale model box [1-3]. In real cases, debris flows triggered by rainfall are frequently confronted. As such, it is of great importance to understand its flowing behaviour and the interaction between solids and fluids bearing inside debris flows. Coupling methods provide an avenue to unveil the multiscale behaviour of debris flows, among which the CFD-DEM method proposed by Tsuji et al. [4, 5] might be the most favoured one. Primarily, Li et al. [6, 7] revealed the interaction between saturated debris flows and flexible structures via the divided void fraction scheme as stated in [8, 9]. Following these, Kong et al. [10] further applied the CFD-DEM method in a real case. A thorough perspective about the generation of the dead zone and the impact of debris flows on flexible barriers is also given in [11] and [12], respectively. Zhao et al. also studied the moving transition process of submerged debris flows with the unresolved CFD-DEM method. In addition to the impact on engineering structures and flowing behaviour itself, debris flows also entrain a great number of masses that exaggerate damage during moving. Zheng et al. [13] discussed the effect of viscous shear flows on the entrainment of debris flows using the unresolved CFD-DEM method. Up to date, most of the numerical studies treated the basal as rigid or uniformly graded. However, the fabric of basal particles is known to be gap-graded under some circumstances, in which boulders might be entrained along the path debris flows passed by. Conventional CFD-DEM coupling schemes like the coarse grid method might not be suitable for gap-graded issues as the ratio of fluid cells to particle diameter shall be smaller than at least 1/3 [14]. To tackle the situation where particle diameter might be equal or larger than fluid cells, Jing et al. [15] put forward the big-particle model and compared it with the previous divided model.

In this work, a semi-resolved coupling scheme based on diffusion averaging is also utilised to ease gap-graded problems. Unlike the counterpart of unresolved schemes, in semi-resolved schemes, particle fraction around a single particle is determined through a kernel function other than constant [14, 16]. After benchmarking the model, debris flows are then described in a representative element with periodic boundaries. Erodible sand basal is modelled with DEM here and the rheological behaviour of debris fluids is governed via a non-Newtonian model.

2. CFD-DEM computational approach

Within the CFD-DEM framework, the motion of a particle is ruled by Newton's second law:

$$m_i \frac{d\mathbf{v}_i}{dt} = \sum_j \mathbf{F}_{ij} + \mathbf{F}_{f-s} + m_i\mathbf{g} \tag{1}$$

$$I_i \frac{d\boldsymbol{\omega}_i}{dt} = \sum_j \mathbf{M}_{ij} + \mathbf{M}_{f-s} \tag{2}$$

where m_i is the mass of particle i-th, $\mathbf{v}_i$ is the particle velocity at this timestep, $\mathbf{g}$ is the gravity acceleration, $\mathbf{F}_{ij}$ is the fluid-solid interaction forces, I_i is the moment of inertia of particle i-th, ω_i is the rotational velocity of particle i-th, $\mathbf{M}_{ij}$ and $\mathbf{M}_{fs}$ indicate the moment resulted from particle collision and fluids, correspondingly. The Hertzian-Mindlin contact rule is utilised herein to describe the force-displacement relationship of contacts in DEM. The normal force for two particles in contact is calculated by the following equations:

$$F_{ij}^n = \frac{4}{3} E_e R_e^{1/2} \delta_n^{3/2} \tag{3}$$

$$F_{ij}^d = \beta_d v_{ij} \tag{4}$$

$$\beta_d = -2\sqrt{\frac{5}{6}}\frac{\ln(e_c)}{\left(\ln(e_c)+\pi^2\right)^{1/2}}\left(2m_e E_e \left(R_e \delta_n\right)^{1/2}\right)^{1/2} \tag{5}$$

where F_{ij}^n is the normal contact force between i^{th} and j^{th} particles, E_e is the effect modulus, R_e is the effective radius, δ_n is the normal relative displacement between i^{th} and j^{th} particles, F_{ij}^d presents the damping force, v_{ij} is the relative velocity between i^{th} and j^{th} particles and β_d is obtained via Eq. (5). It is noted that value of β_d is chiefly controlled by the restitution coefficient e_c. Particles are allowed to rotate free in this study. To take account for irregular particle shape, the rolling resistance contact element is involved. The torque exerted on the particle i can be obtained via the following equation:

$$T_{ij} = -\frac{\varpi_{ij}}{\left|\varpi_{ij}\right|}\mu_r R_e F_{ij}^n \tag{6}$$

where T_{ij} is the torque induced by the rotation between particles i^{th} and j^{th}, μ_r is the rolling resistance coefficient. As to fluid-solid interacting forces, earlier studies have illustrated that, for debris flows, drag force and hydrostatic force dominate the impact of fluids on particles, while other terms of interaction force can be negligible [17]. Thus, two forces are accounted for in the system and they are expressed as:

$$\mathbf{F}_{f-s} = \mathbf{F}_d + \mathbf{F}_{\nabla p} \tag{7}$$

As to the solving of fluid phases, due to the existence of free surfaces in debris flows, the volume of fluids (VOF) method is implemented to determine the interface between the air and debris fluids. The phase evolution between two fluids is determined via the advection equation:

$$\frac{\partial \varepsilon_f \alpha_i}{\partial t} + \nabla\cdot\left(\varepsilon_f \alpha_i \mathbf{u}_f\right) - \nabla\cdot\left(\mathbf{u}_c \varepsilon_f \alpha_i \alpha_j\right) = 0 \tag{8}$$

where $\mathbf{u}_c$ indicates the compression velocity, α_i is the volume fraction of fluid i and α_j the volume fraction of fluid j. Both volume fractions are constrained by:

$$\alpha_j = 1 - \alpha_i \tag{9}$$

Thus, volume-averaged Navier-Stokes equations are defined as:

$$\frac{\partial}{\partial t}\left(\varepsilon_f \rho_f\right) + \nabla\cdot\left(\varepsilon_f \rho_f \mathbf{u}_f\right) = 0 \tag{10}$$

$$\frac{\partial}{\partial t}\left(\varepsilon_f \rho_f \mathbf{u}_f\right) + \nabla\cdot\left(\varepsilon_f \rho_f \mathbf{u}_f \otimes \mathbf{u}_f\right) = -\varepsilon_f \nabla p + \nabla\cdot\left(\varepsilon_f \mu \nabla \mathbf{u}_f\right) + \varepsilon_f \rho_f \mathbf{g} + \varepsilon_f \mathbf{F}_\sigma + \mathbf{F}_d \tag{11}$$

where ε_f is the fluid volume fraction. It can be seen that only drag force and hydrostatic force is maintained. The surface tension force is calculated based on the fluid fraction solved in Eq. (8)

$$F_\sigma = \sigma\kappa\nabla\alpha \tag{12}$$

$$\kappa = \nabla\cdot\left(\frac{\nabla\alpha}{\left|\nabla\alpha\right|}\right) \tag{13}$$

where σ is the surface tension and κ is the two-phase interface curvature. In the semi-resolved CFD-DEM scheme, particle fraction of a fluid cell can be specified through the expression below:

$$\varepsilon_p = 1 - \frac{\sum_{i=1}^{N_p}\varepsilon_p^i V_p^i}{\Delta V_p} \tag{14}$$

where $V_{p,i}$ is the volume of particle i, ΔV_p presents the volume of the fluid cell and ε_p^i is the particle fraction induced by particle i residing in the cell [18]. A diffusion equation can be used to solve the particle fraction ε_p^i as follows:

$$\frac{\partial \varepsilon_p^i}{\partial t} = \frac{l^2}{\Delta t} \nabla^2 \varepsilon_p^i \tag{15}$$

where l represents a characteristic averaging length scale [19]. The particle fraction distribution of a single particle is presented in Fig. 1, in which the particle fraction at neighbouring fluid cells follow the solution of the diffusion equation.
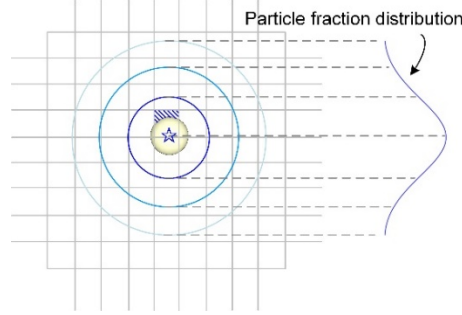
Fig. 1. The paradigm of averaging particle fraction distribution.

Regards of the nonlinear behaviour of debris fluids, some non-Newtonian rheological models such as the HB model and the Bingham model have been implemented in the literature. However, artificial viscosity is required to avoid the singularity when the shear strain rate gets close to zero [20, 21]. Therefore, a promoted HB model in which numerical divergence can be prevented has been proposed [22]. The generalised shear stress τ can take the form:

$$\tau = \mu_{eff} \dot{\gamma} \tag{16}$$

where μ_{eff} is the effective viscosity and $\dot{\gamma}$ is the shear strain rate. The effective viscosity in Eq. (16) can be further formulated as:

$$\mu_{eff} = \frac{\mu_d \left(2\dot{\gamma}\right)^n + \tau_y \left(1 - e^{-m\dot{\gamma}}\right)}{\dot{\gamma}} \tag{17}$$

where m and n are two model parameters and keep constant during calculation; μ_d and τ_y are the dynamic viscosity and yield stress, respectively. Then, substituting Eq. (17) to Eq. (16), the fluid stress τ can be derived as:

$$\tau = \mu_d \left(2\dot{\gamma}\right)^n + \tau_y \left(1 - e^{-m\dot{\gamma}}\right) \tag{18}$$

The two parameters m and n take charge of fluid behaviour. When $n = 1$, the HBP model degenerates into the BP model [23]. Under the increasing shear strain rate, the HBP model can be transformed into the HB model. For those who take an interest in the details of the HBP model, some other researches have indicated a more comprehensive explanation of its behaviour which may not be repeated here [20, 21, 24]. In this study, HBP model is implemented in the open-source CFD code OpenFOAM with C++.

3. Numerical Applications

3.1. Model verification

The performance of the semi-resolved scheme is evaluated via the classical case of single-particle settlement in water. The parameter settings are borrowed from [9]. Particle velocity obtained from the analytical solution and the semi-resolved model is compared in Fig. 2. Definitely, the particle velocity trend in the model agrees well with the analytical solution. At first, the particle accelerates linearly driven by gravity. Then, the particle falls into the water and slow down. Finally, the particle velocity keeps steady until touching the base. In the model, the particle velocity oscillates after contacting the base since its kinetic energy has not been fully dissipated during falling so it bounces back.
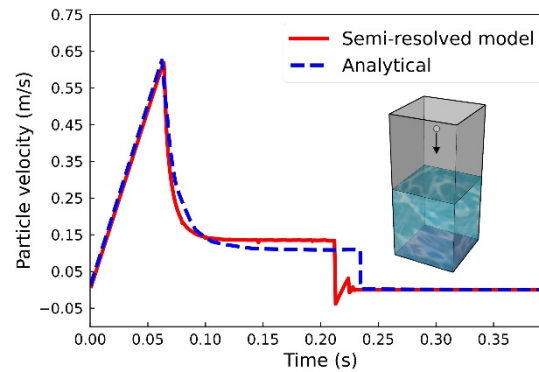
Fig. 2. Particle velocity versus time: comparison between the semi-resolved model (solid line) and the analytical solution (dotted line).

The flume experiment on water-kaolinite clay mixtures performed by Komatina et al. [25] is simulated to verify the availability of the HBP model implemented in CFD code. Parameters utilised in the HBP model is derived from [20], in which the same experiment was used for validation. Fig. 3 illustrates the setup and boundary conditions of the flume test. The channel has a length of 4000 mm and a height of 200 mm. The motion of fluids starts after removing the constraint at the middle of the model. Kaolinite clay is modelled with pure CFD code as the instance is utilised to verify the implemented HBP model. Fig. 4 compares the numerical and experimental flowing patterns at 0.37 s and 0.60 s. It is evident that the propagation distance of clay mixtures can be fairly predicted with the implemented model.
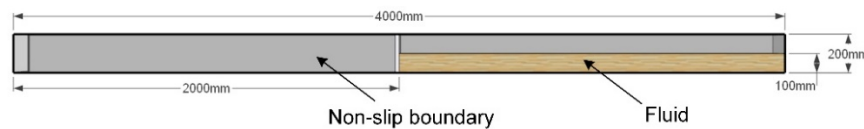
Fig. 3. The flume model setup, where the fluid indicates the clay mixtures used in the experiment, after [25].
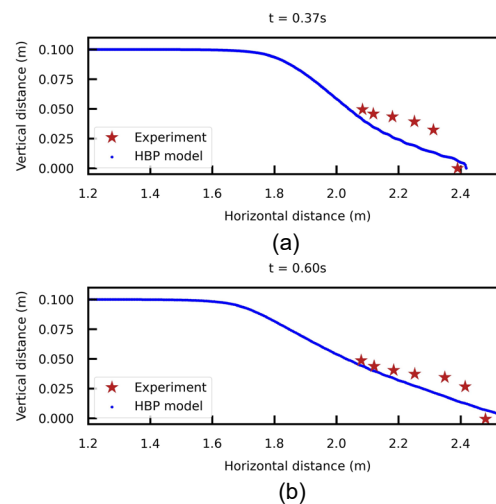

Fig. 4. Lateral fluid contour comparison with the HBP model and the experiment: (a) $t = 0.37$ s and (b) $t = 0.60$ s.

3.2. Dam break with erodible basal

3.2.1. Dam break model setup

5

After validating the semi-resolved scheme and the HBP model, the debris flow model containing erodible basal and debris fluids is indicated in Fig. 5, where the flowing behaviour of fluids is described with the HBP model. The model geometry is defined as a box with 500 mm width, 100 mm thickness and 300 mm height. Erodible basal is composed of non-cohesive particles and collision behaviour is yielded via the Hertz model as mentioned in Section 2. The periodic boundary is applied in the thickness dimension to remove the size effect, while the atmospheric condition is used in the top boundary. The non-slip boundary is exerted on other faces of the model box. The model mesh size is 10 mm, which is appropriate for CFD-DEM analyses in this case. Finer meshes can bring higher resolution of fluid interfaces, but it might result in degradation in computational efficiency.
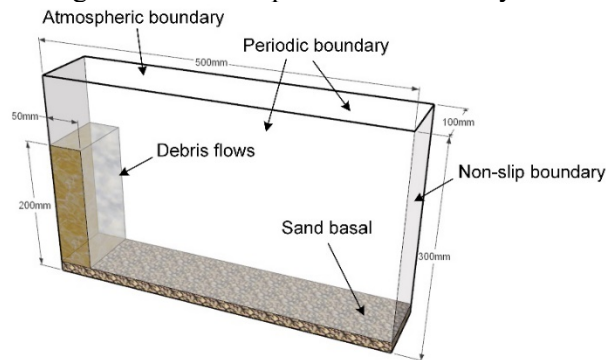
Fig. 5. Diagram of the debris flow model with the erodible sand basal.
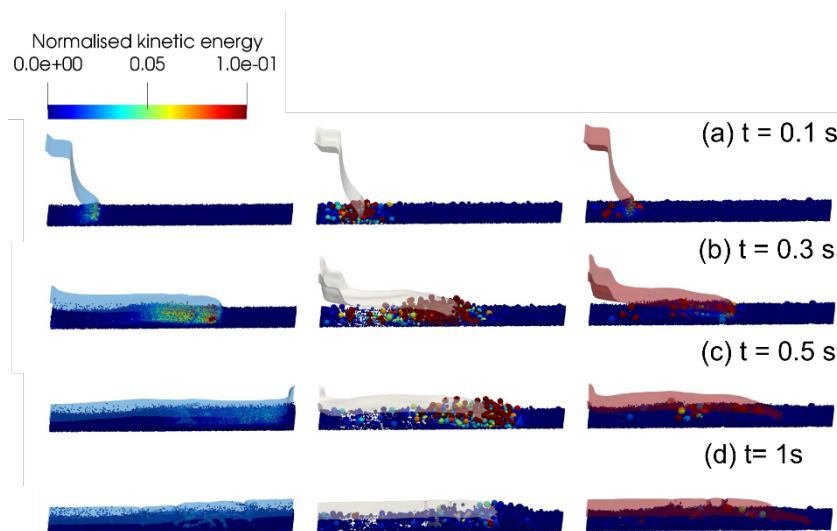
Three typical sets of particle size distribution are used in basal manipulation to study the effect of gap-graded basal on entrainment results. The first basal sample has monodispersed particles of 3 mm diameter, while the second one is properly graded with $C_u = 5$ and $C_s = 1.8$. Gap-graded particles are applied in the third model, in which $C_u < 5$. For each test, the total simulated real time is 1 s.

$$C_u = \frac{d_{60}}{d_{10}} \tag{19}$$

$$C_s = \frac{d_{30}^2}{d_{60} d_{10}} \tag{20}$$

where d_{60} is the particle size at which 60% of the particles are finer and the same rule for d_{30} and d_{10} [26]. A shear-thickening fluid is used to simulate the behaviour of debris flows, in which $m = 0.20$ and $n = 1.5$ being used in the HBP model.

3.2.2. Entrainment process

Fig. 6. Progressive entrainment under three types of basal with different particle size distribution.

After removing the lateral confinement of debris fluids, debris flows entrain particles containing in the basal and continue flowing with fluid-particle mixtures. The entrainment process of three tests having varied size distribution is demonstrated in Fig. 6. The left column presents the basal with monodispersed grading. The middle one has the properly graded particle size distribution, while the counterpart of the right column is gap-graded. Initially, the debris fluid columns collapse in a similar style. Then, debris flows move quicker in the monodispersed basal than the other two cases, in which properly graded basal owns the smallest propagation distance. This mechanism can be also reflected on the normalised kinetic energy field. For the properly graded case, larger particles of the basal have much higher kinetic energy in contrast to others. Boulders existing in the basal carry most of the kinetic energy as to the gap-graded case. Therefore, the monodispersed particles possess less kinetic energy and more potential energy bearing in the initial debris flows being transferred into the fluids.

4. Conclusions

In this paper, the numerical framework takes advantages of the semi-resolved CFD-DEM method and a non-Newtonian rheological model with convergence at the infinitesimal shear strain rate. After validation, the method is utilised to simulate the entrainment resulted from debris flows. Then, the responses of three types of basal to debris flows are analysed, in which each owning different particle size distribution. Through comparing these tests, particle size appears to have an important effect on final deposition patterns. It is emphasized that, in contrast to the basal consisting of monodispersed particles, the propagation distance can be decreased for those having larger particles. However, the entrained large particles are observed to contain a much higher kinetic energy, which may threaten engineering structures.

5. Acknowledgement

References

[1]   R. M. Iverson, M. E. Reid, M. Logan, R. G. LaHusen, J. W. Godt, and J. P. Griswold, "Positive feedback and momentum growth during debris-flow entrainment of wet bed sediment," *Nature Geoscience,* vol. 4, no. 2, pp. 116-121, 2010.

[2]   R. M. Iverson, "Scaling and design of landslide and debris-flow experiments," *Geomorphology,* vol. 244, pp. 9-20, 2015.

[3]   C. W. W. Ng, C. E. Choi, D. K. H. Cheung, and Y. Cui, "Effects of dynamic fragmentation on the impact force exerted on rigid barrier: centrifuge modelling," *Canadian Geotechnical Journal,* vol. 56, no. 9, pp. 1215-1224, 2019.

[4]   Y. Tsuji, T. Tanaka, and T. Ishida, "Lagrangian numerical simulation of plug flow of cohesionless particles in a horizontal pipe," *Powder Technology,* vol. 71, no. 3, pp. 239-250, 1992.

[5]   Y. Tsuji, T. Kawaguchi, and T. Tanaka, "Discrete particle simulation of two-dimensional fluidized bed," *Powder Technology,* vol. 77, no. 1, pp. 79-87, 1993.

[6]   X. Li, J. Zhao, and J. S. H. Kwan, "Assessing debris flow impact on flexible ring net barrier: A coupled CFD-DEM study," *Computers and Geotechnics,* vol. 128, 2020.

[7]   X. Li and J. Zhao, "A unified CFD-DEM approach for modeling of debris flow impacts on flexible barriers," *International Journal for Numerical and Analytical Methods in Geomechanics,* vol. 42, no. 14, pp. 1643-1670, 2018.

[8]   T. Shan and J. Zhao, "A coupled CFD-DEM analysis of granular flow impacting on a water reservoir," *Acta Mechanica,* vol. 225, no. 8, pp. 2449-2470, 2014.

[9]   J. Zhao and T. Shan, "Coupled CFD–DEM simulation of fluid–particle interaction in geomechanics," *Powder Technology,* vol. 239, pp. 248-258, 2013.

[10]   Y. Kong, J.D. Zhao, X.Y. Li, J.S.H. Kwan, and E. C. H. Sze, "Coupled CFD/DEM Modeling of Multiphase Debris Flow over a Natural Erodible Terrain: the Yu Tung Road Case," presented at the Second JTC1 Workshop on Triggering and Propagation of Rapid Flow-like Landslides, Hong Kong, 2018.

[11]   Y. Kong, J. Zhao, and X. Li, "Hydrodynamic dead zone in multiphase geophysical flows impacting a rigid obstacle," *Powder Technology,* 2021.

[12]   Y. Kong, X. Li, and J. Zhao, "Quantifying the transition of impact mechanisms of geophysical flows against flexible barrier," *Engineering Geology,* vol. 289, 2021.

[13]   H.-C. Zheng, Z.-M. Shi, M. Peng, and S.-B. Yu, "Coupled CFD-DEM model for the direct numerical simulation of sediment bed erosion by viscous shear flow," *Engineering Geology,* vol. 245, pp. 309-321, 2018.

[14]   Z. Wang, Y. Teng, and M. Liu, "A semi-resolved CFD–DEM approach for particulate flows with kernel based approximation and Hilbert curve based searching strategy," *Journal of Computational Physics,* vol. 384, pp. 151-169, 2019.

[15]   L. Jing, C. Y. Kwok, Y. F. Leung, and Y. D. Sobral, "Extended CFD-DEM for free-surface flow with multi-size granules," *International Journal for Numerical and Analytical Methods in Geomechanics,* vol. 40, no. 1, pp. 62-79, 2016.

[16]   R. Sun and H. Xiao, "Diffusion-based coarse graining in hybrid continuum–discrete solvers: Theoretical formulation and a priori tests," *International Journal of Multiphase Flow,* vol. 77, pp. 142-157, 2015.

[17]   T. Zhao, S. Utili, and G. B. Crosta, "Rockslide and Impulse Wave Modelling in the Vajont Reservoir by DEM-CFD Analyses," *Rock Mechanics and Rock Engineering,* vol. 49, no. 6, pp. 2437-2456, 2015.

[18]   S. Kuang, M. Zhou, and A. Yu, "CFD-DEM modelling and simulation of pneumatic conveying: A review," *Powder Technology,* vol. 365, pp. 186-207, 2020.

[19]   M. Vångö, S. Pirker, and T. Lichtenegger, "Unresolved CFD–DEM modeling of multiphase flow in densely packed particle beds," *Applied Mathematical Modelling,* vol. 56, pp. 501-516, 2018.

[20]   Z. Han *et al.*, "Numerical simulation of debris-flow behavior based on the SPH method incorporating the Herschel-Bulkley-Papanastasiou rheology model," *Engineering Geology,* vol. 255, pp. 26-36, 2019.

[21]   Z. Han, B. Su, Y. Li, J. Dou, W. Wang, and L. Zhao, "Modeling the progressive entrainment of bed sediment by viscous debris flows using the three-dimensional SC-HBP-SPH method," *Water Res,* vol. 182, p. 116031, Sep 1 2020.

[22]   T. C. Papanastasiou, "Flows of Materials with Yield," *Journal of Rheology,* vol. 31, no. 5, pp. 385-404, 1987.

[23]   B. Domnik and S. P. Pudasaini, "Full two-dimensional rapid chute flows of simple viscoplastic granular materials with a pressure-dependent dynamic slip-velocity and their numerical simulations," *Journal of Non-Newtonian Fluid Mechanics,* vol. 173-174, pp. 72-86, 2012.

[24]   G. Fourtakas and B. D. Rogers, "Modelling multi-phase liquid-sediment scour and resuspension induced by rapid flows using Smoothed Particle Hydrodynamics (SPH) accelerated with a Graphics Processing Unit (GPU)," *Advances in Water Resources,* vol. 92, pp. 186-199, 2016.

[25]   D. Komatina and M. Jovanovic, "Experimental study of steady and unsteady free surface flows with water-clay mixtures," *Journal of Hydraulic Research,* vol. 35, no. 5, pp. 579-590, 1998.

[26]   T. Allen, "4 - Particle size analysis by sieving," in *Powder Sampling and Particle Size Determination*, T. Allen, Ed. Amsterdam: Elsevier, 2003, pp. 208-250.